# Mechanical Design Optimization of a Piping Inspection Robot

Damien Chablat, Swaminath Venkateswaran, Frédéric Boyer

# Mechanical Design Optimization of a Piping Inspection Robot

Damien Chablat[1], Swaminath Venkateswaran[2], Frédéric Boyer [3]
[1]CNRS, Laboratoire des Sciences du Numérique de Nantes (LS2N),
UMR CNRS 6004, 1 rue de la Noë, 44321 Nantes, France
[2]École Centrale de Nantes, Laboratoire des Sciences du Numérique de Nantes (LS2N),
UMR CNRS 6004, 1 rue de la Noë, 44321 Nantes, France
[3]IMT Atlantique, Laboratoire des Sciences du Numérique de Nantes (LS2N),
UMR CNRS 6004, 4 rue Alfred Kastler La Chantrerie, 44307 Nantes,France

April 23, 2018

**Abstract**

*The piping inspection for security or sealing checking is an important challenge when the internal diameter of the pipe is small with respect to its length. Some mechanisms using closed loops are able to generate contact forces and deployable structures. By using bio-inspired design, we present a mechanism which is able to move inside pipes by mimicking the motion of a caterpillar. The mechanism is composed of three sections, one for the motion and two with legs that are attached with the inner part of the pipe. A compliant mechanism is proposed to add mobility between the three sections of the robot in order to cross the singularity of the pipe. The results coming from a multi-objective optimization process is used to set the geometric and kinematic parameters of the mechanism taking into account the environmental and design constraints. A mechatronic system is proposed that uses industrial components namely DC motors, ball-screws and servo controllers which can be inserted in the pipe. For horizontal and vertical motions, the contact forces and the motor torques are computed to check the feasibility of the clamping. A prototype made at Laboratoire des Sciences du Numérique de Nantes (LS2N) is used to show the behavior of this concept for slow motions.*
**Keywords:** Bio-Inspired Design; Robot; Kinematics; Piping Inspection

## 1 Introduction

Nuclear power plants employ pipeline equipments which are sometimes difficult to be accessed by human beings due to radiation issues and inaccesible zones. In order to perform a quality check (or) inspection in such regions, robotic devices are employed which reduces human intervention and prevents the loss of human life. At present, there are many piping inspection robots which are used in Nuclear and Chemical plants pipelines. The locomotion system of such robots can be imagined by using mechanical devices or bio-ispired techniques. Kassim et al. proposed a distinction between the two categories of locomotion systems [1]. Some of the existing robots with mechanical locomotion systems employ wheels and pulleys [2], telescopic [3], impact [4] (or) natural peristalsis [5]. Some of the bio-inspired robots use locomotion principles that are mimicked from earthworms [6], snakes [7], millipedes [8], lizards [9] (or) an octopus [10]. However, a pipeline inspection robot is encountered by four main problems namely: (i) locomotion (or) movement of the system due to variation of pipe diameters, elbows (or) bends and orientation of pipeline (ii) accurate positioning of the robot inside the pipeline, (iii) inspection of the pipeline by the robot with effective communication system between the monitoring device and on-board sensors and (iv) perform mechanical tasks (welding, cleaning etc.) by withstading the vibrations and other forces generated by the machines mounted on the robot. In this article, we focus on the locomotion principle and working of a bio-inspired robot that mimics the motion of a caterpillar that has been presented by Henry et al [11]. The robotic system is subdivided into three mechanisms: one for the locomotion and two leg mechanisms for adaptive contact points with the interior walls of the pipeline. Three architectural candidates for the leg mechanism namely: the slot follower, the 4 bar follower crank and the 6 bar follower crank mechanisms were taken into study for optimization [11]. Optimization technqiues can be classified into Deterministic and Heurisitc apporaches where the latter is more efficient and flexible with reduced computational times [12]. A multi-objective optimization using Genetic algorithm (Heuristic approach) is employed to determine the optimal leg mechanism for the robot. DC motors are used in the system for actuation over pneumatic systems owing to the presence of dust particles and contamination issues inside nuclear power plant pipelines. However, the study of forces and torques on the motors used in the robot were not done in detail which is very essential to understand the robustness of the system under various inclinations and obstacles faced within the pipeline. A static force analysis using a Coulomb model is

presented which helps in determining the clamping forces as well as the forces induced on the motors in the robot while moving inside pipelines of varying diameters and inclinations.

The outline of the paper is as follows. The locomotion principle of the bio-inspired robot is presented. Followed by that, an overview of the optimization results of the leg mechanism used in the system is presented. A 3D model of the entire system using CATIA as well as the prototype made at LS2N is provided in the subsequent section. Finally, the results of static analysis of the robot are presented in order to understand the contact forces of the robot with the wall during horizontal and vertical travels as well as a function of its orientation inside the pipeline. The paper then ends with closing conclusion and remarks.

## 2 Locomotion of the system

The locomotion of the system is inspired from the motion of a caterpillar. The locomotion comprises of three steps: one for blocking and two others for elongation. A classic way to accomplish this would be with the help of pneumatic bellows for blocking and electric motors for the elongation [13, 14] but this solution is not feasible in a nuclear power plant owing to dust and contamination issues. A typical motion of a caterpillar is depicted in Fig. 1. Using actuators, the locomotion is successfully mimicked in the system under study. A cross-sectional view of the robot is presented in Fig. 2.

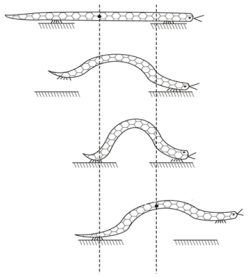

Figure 1: Typical locomotion of a caterpillar [15]

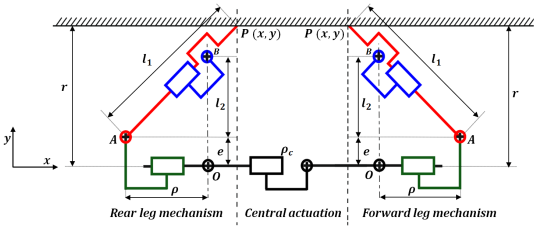


Figure 2: Cross section of the robot inside a pipeline of radius $r$

Three linear actuators are used in the system in order to achieve locomotion. The central actuator represented by $\rho_c$ in Fig. 2 is used for the elongation. $O$ is the origin (or) the reference point for the leg mechanism. The prismatic joint is represented by $OA$ and the stroke length of the actuator used in legs is $\rho$. Three leg modules are mounted with a phase shift angle of 120 ° at a distance $e$ from the central axis of the robot. The length of the slider corresponds to $l_1$ and the sliding point distance between $A$ and $B$ is denoted by $l_2$. At least one set of legs (forward or rear) of the robot remains in contact at all times with the walls of the pipeline. A hyper-static posture exists when both the set of legs of the robot are in contact with the walls. Two motors, one for the rear and one for the forward leg mechanisms are used in order to fix the robot with the internal radius of the pipeline $r$. Similar to the motion of a caterpillar, the motion of the robot inside the pipe is accomplished in six steps which is depicted in Fig. 3. The legs of the robot

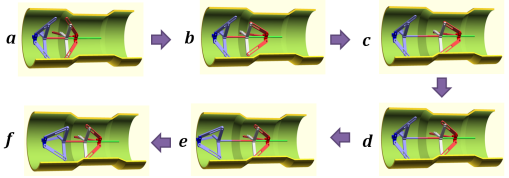


Figure 3: Six step locomotion of the robot inside a pipe with variable diameters

can adapt their stretch based on the changes in diameter encountered within the pipeline. The radius of the pipelines under study ranges from a superior $r_{max}$= 37 mm to a minimum $r_{min}$= 27 mm. Taking into account the actuation of the system, the legs are mounted at an offset of 11 mm from the central axis. Thus, the target radius to be swept by the legs are now reduced to $r_{max}$= 26 mm and $r_{min}$= 16 mm. A simulation result of the locomotion of the robot inside the pipeline is shown in Fig. 4.

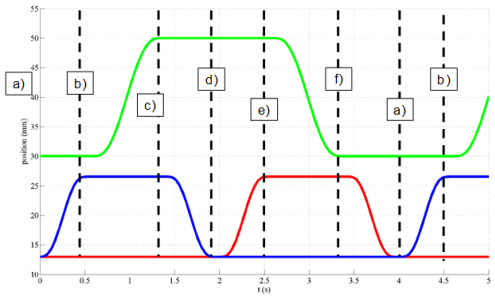


Figure 4: Position of the joints/actuators of the robot during a locomotion cycle

The green line depicts the movement of the central actuator at various instances of time. The red and blue line depicts the actuators of the forward and the rear leg mechanisms, respectively. A hyper-static mode exists when the blue and red lines meet at a particular position i.e. when both the legs are in contact with the walls. For crossing a diameter change, there is a delay between the two clamping modules. This is explained by the fact that it is necessary to wait at least one cycle of locomotion so that the two modules are on the same diameter. The simulation result of locomotion with diameter changes inside the pipeline is shown in Fig. 5.

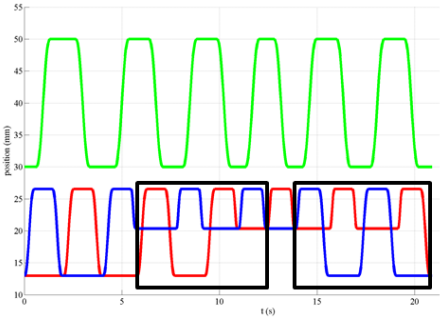


Figure 5: Position of the joints/actuators of the robot during diameter change

The highlighted black boxes represent the positions of the rear and forward actuators when the inner diameter decreases for the first box and then increases for the second one. This property enables us to design the robot with a static analysis.

# 3 Optimization results of the slot follower leg mechanism

Three leg mechanisms were taken into study and was modeled using MAPLE for extracting the geometric models. With the help of Genetic algorithm in MATLAB [16], the slot follower mechanism [17, 18, 19] was chosen as it provided the maximum transmission force with minimal space over the other two architectures [11]. Using MAPLE, the direct and the inverse kinematic problem (DKP and IKP) for the mechanism is derived and the relations are given by:

$$\text{DKP:} \qquad P_y = \frac{l_2^2 e + \rho^2 e + \sqrt{l_1^2 l_2^4 + l_1^2 l_2^2 \rho^2}}{l_2^2 + \rho^2} \tag{1}$$

$$\text{IKP:} \qquad \rho = \frac{l_2 * \sqrt{l_1^2 - e^2 + 2eP_y - P_y^2}}{P_y - e} \tag{2}$$

The distance $e$ is 11 mm from the central axis of the robot, which is a constraint imposed by the dimensions of the motor used for the leg mechanisms. The mechanical limits for this mechanism are given by $y_{max}$=$l_1$ and $y_{min}$=$l_2 + e$. A serial singularity occurs when $O$ and $A$ (Fig. 2) coincides. A multi-objective optimization using genetic algorithm was carried out in order to minimize the size of the mechanism and to maximize the transmission force. The inverse

kinematic model is used to satisfy the first objective i.e., minimize the size of the mechanism subject to varying diameters of the pipeline. Using MAPLE, the Jacobian and inverse Jacobian was estimated. The latter serves as the second objective that maximizes the transmission force. The inverse Jacobian provides the force transmission factor which is given by:

$$\eta_f = \frac{(\rho^2 + l_2^2)^{3/2}}{l_2 l_1 \rho} = \frac{F_p}{F_a} \tag{3}$$

Here $F_a$ represents the actuation force of the motor and $F_p$ signifies the contact forces between the legs of the robot and the walls of the pipeline. A Pareto front was generated after optimization with the help of which the optimal results for the system is extracted. An intermediate solution was chosen in [11] from the Pareto front in order to have a better compromise of the final results. The dimensions of the leg mechanism used in the system is provided in Table 1.

Table 1: Optimized dimensions of the slot-follower leg mechanism

| **Lengths** | **Dimensions** $[mm]$ |
|---|---|
| $l_1$ | 57 |
| $l_2$ | 7 |
| $e$ | 11 |
| $\rho$ | 8.5-45.5 |

# 4 Static analysis on the robot

With the results of the optimization of the leg mechanism, the complete robotic system which mimics the motion of a caterpillar is modeled using CATIA. The rendered model of the robotic system in CATIA and the prototype of the robot made at LS2N are shown in Fig. 6 and Fig. 7.

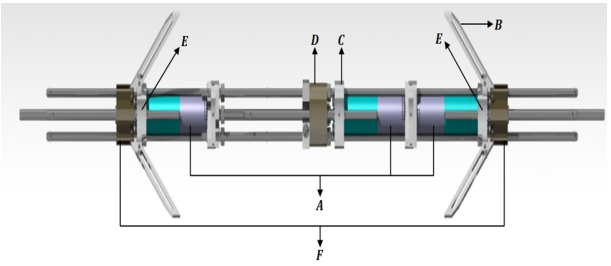


Figure 6: Rendered model of the robot in CATIA

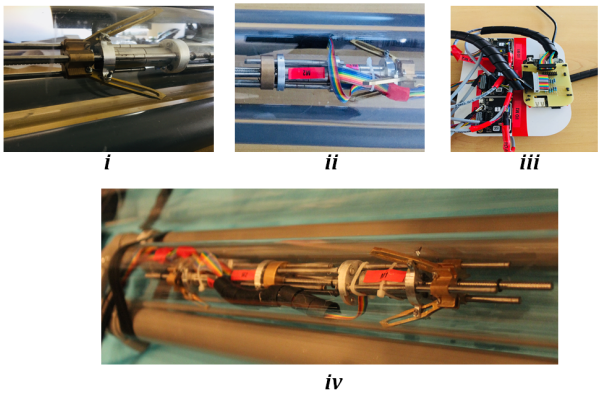


Figure 7: Protoype of the robot made at LS2N

In Fig. 7, (i) represents the leg mechanism of the robot, (ii) represents the central actuation system along with the other leg mechanism, (iii) represents the electronic control board used for the robot and (iv) represents the entire robotic system inside the pipeline. The robot is a multi-body mobile-based system with closed loops. The three legs

of the rear and forward mechanisms have the same dimensions and they ensure non-hyper-static contacts at almost all phases of the locomotion. The motors used for the central actuation of the robot as well as for the leg mechanisms is a Maxon motor GP 16 S ($\phi$16) [20]. Each module has its own motor system. The gear ratio offered by this motor is 1:455 (Nominal torque of 1.5 N.m). The details of material and individual masses of the motor, the legs and the flanges used are provided in Table 2.

Table 2: Mass properties of Flanges, Motor and Legs of the robot from Fig. 6

| **Component** | **Material** | **Mass** $[g]$ | **Quantity** |
|---|---|---|---|
| Maxon motor GP 16 S (A) | X46Cr13 | 69 | 3 |
| Slot-follower legs (B) | Bronze | 2 | 6 |
| Central motor locking flange (C) | Aluminium | 11 | 1 |
| Central flange (D) | Bronze | 13 | 1 |
| Leg motor locking flange (E) | Aluminium | 13 | 2 |
| Locking screws for legs (F) | Bronze | 41 | 2 |

The complete assembly other than the parts provided in Table 2 includes steel fasteners such as screws, nuts and circlips with the help of which the entire robotic system is realized. The entire mass of the robotic system is 657 g not taking into account the electornic boards and wiring units. An ESCON 36/3 DC servo-controller (Torque and speed control) [20] is used in the robot for an efficient control of the DC motors used for actuation. The torque on the motor can be calculated in two phases: a dynamic algorithm during locomotion and a static algorithm during clamping. Only the static algorithm during clamping will be discussed in this paper. An unknown force will be applied on the robot during motion by the umbilicus due to its mass and friction with the walls. The umbilicus used in the system has a weight span of around 56 N per 100 m (Copper cables) and it imposes a mass on the robot. While passing through curved sections or elbows there exists frictional forces between cables and walls and it increases as the bend angle goes from 0 to 90 °. However, only through experiments, we can calculate these unknown forces.

## 4.1 Static algorithm- Estimation of motor torques and forces

In this section, the robot is assumed to be made by a beam with a punctual mass connected to a wall by three points. We look for a contact force between the pipe and the legs that respects the Coulomb's law of friction. For every contact point, the forces can be broken down into:

- $N_i$ - Normal Force
- $T_{li}$ -Tangential longitudinal Force
- $T_{ri}$ -Tangential radial Force

A schema of these forces inside a pipeline of radius $r$ is shown in Fig. 8 .

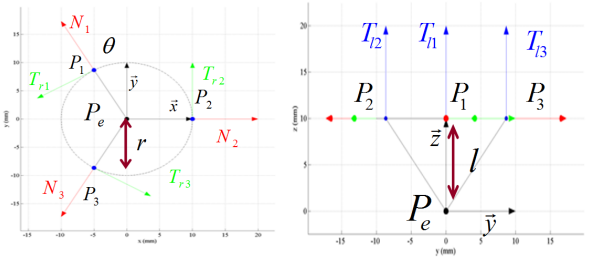


Figure 8: Schema of the contact forces during clamping as seen in $x-y$ (left) and $y-z$ (right) planes

We have three parameters for the leg module in which the parameters $l$ and $r$ determines the contact circle and the parameter $\theta$ determines the rotation of the legs. The contact points are represented by $P_1$, $P_2$ and $P_3$ and the center point is represented by $P_e$. The vector equations are given by:

$$P_e = \begin{pmatrix} 0 \\ 0 \\ 0 \end{pmatrix} \tag{4}$$

$$P_{1,2,3} = \begin{pmatrix} r\cos\left(\frac{2\pi j}{3}\right) \\ r\sin\left(\frac{2\pi j}{3}\right) \\ l \end{pmatrix} \quad \text{where} \quad j = 0, 1, 2 \tag{5}$$

About the center point $P_e$, there exists a wrench which is given by the equation:

$$T_e = \begin{pmatrix} R_x & M_x \\ R_y & M_y \\ R_z & M_z \end{pmatrix} \tag{6}$$

The effort about the central point is calculated using a dynamic model. Under static conditions, the equilibrium equations are given by:

$$\sum R_i = 0 \ \& \ \sum M_i = 0 \tag{7}$$

The contact forces between the walls of the pipeline and the legs of the robot provides the reaction forces which is essential to compute the longitudinal and radial forces. The wrench equation at the three contact points is given by:

$$T_{ii} = \begin{pmatrix} \{R\} \\ \{M\} \end{pmatrix} = \begin{pmatrix} T_{ri}\cos\left(\frac{2\pi j}{3} + \frac{\pi}{2}\right) & 0 \\ T_{ri}\sin\left(\frac{2\pi j}{3} + \frac{\pi}{2}\right) & 0 \\ T_{li} & 0 \end{pmatrix} \tag{8}$$

$$\text{where } j = 0, 1, 2 \text{ and } i = 1, 2, 3$$

Using the Varignon's theorem, the wrench with respect to the central point is calculated based on the relation:

$$T_{i_0} = T_{ii} + \vec{R} \times \vec{P}_{i_0} \tag{9}$$

Owing to the frictional contacts between the legs of the robot and the walls of the pipeline, by Coulombs law we have:

$$N_i \geq \frac{\sqrt{T_{ri}^2 + T_{li}^2}}{\varphi} \quad \text{where } i = 1, 2, 3 \tag{10}$$

Here $\varphi$ is the co-efficient of friction between the walls of the pipeline and the legs of the robot. A value of 0.4 is taken between the bronze legs of the robot and the steel walls of the pipeline. Using Eq. 10, the total global force (sum of the normal forces, $N_i$) is estimated. Using Eq. 3 and the global normal force, the forces induced on the actuator is calculated by the relation:

$$F_a = \eta_f N_{total} \tag{11}$$

The above equation determines the force induced within the actuator when the robot establishes a contact with the walls of the pipeline. The actuator force is also affected by the orientation of the pipeline. When the robot is traveling inside a horizontal pipeline and one set of legs is clamped on to the walls, the robot behaves like a cantilever beam with a load at the free end. Here the load indicates the self weight of the robot. This load generates a moment about the x-axis (Fig. 8) with respect to the clamped ends. With the weight being concentrated at the center of gravity of the robot, the distance between the clamped legs of the robot and position of center of gravity is essential to estimate the moment equations used in wrench Eq. 9. Using CATIA, this distance is measured for the two diametrical cases under study (27 mm and 37 mm). In the case of vertical pipelines, irrespective of the clamping of the robot with the walls, only the self-weight of the robot exists and the moments induced are zero. The actuator forces for these two configurations of pipeline are estimated.

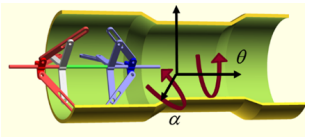


Figure 9: Orientation of the pipeline ($\alpha$) and the robot ($\theta$)

Table 3: Center of gravity position from the clamped legs of the robot

| **Position of Central actuator** | **Radius of the pipeline** ($mm$) | **Position of CG from clamped end**($mm$) |
|---|---|---|
| Initial | 27 | 128 |
| Full extension | 27 | 149 |
| Initial | 37 | 123 |
| Full extension | 37 | 144 |

## 4.2 Results of actuator forces inside horizontal and vertical pipelines

During the static phases, the orientation of the robot ($\theta$) and the orientation of the pipeline ($\alpha$) as shown in Fig. 9 has influences on the motor torque.

The center of gravity (CG) of the robot is also affected by the position of the central actuator. The details about the position of CG from the clamped legs based on central actuation position is provided below in Table 3.

With the help of the wrench Eq. 9 and positions of CG from clamped ends of the robot legs, the longitudinal and radial forces are estimated as functions of the radius of the pipeline $r$, position of the CG from the clamped end $l$ and the self-weight of the robot $P$. The equations are given by:

$$T_{l_{1,2,3}} = f(r, P, l) \tag{12}$$

$$T_{r_{1,2,3}} = f(P) \tag{13}$$

Using MATLAB, the values of the longitudinal, radial and normal forces are estimated using the above equations generated in MAPLE. The results are plotted for these forces with respect to the orientation of the robot ($\theta$). During horizontal positions of the pipeline, the longitudinal forces are mainly affected by the position of the CG from the clamping positions. The results of the forces for 27 mm and 37 mm diameter pipeline with initial and fully extended positions of the central actuator are shown in Fig. 10 and Fig. 11.

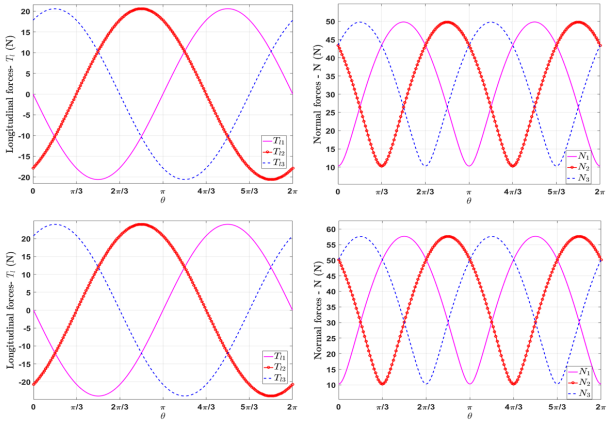


Figure 10: Forces with respect to ($\theta$) in a horizontal pipeline at $r$=27 mm for initial(above) and full extension(below) of central actuator

The radial forces are not affected by the radius of the pipeline or the position of CG and it depends only on the weight of the robot. In the case of vertical orientation of pipeline, only the radial forces exist and it remains the same value as in a horizontal pipeline owing to the weight of the robot $P$. The results of radial forces are: $T_{r_1}$ = 4.6 N, $T_{r_2}$ = -2.3 N and $T_{r_3}$ = -2.3 N for horizontal and vertical orientations of pipeline. The longitudinal forces are zero inside a vertical pipeline as there exists no moments. Normal forces are estimated directly from the radial forces and it remains a constant irrespective of the change in orientation of the robot ($\theta$). With the contact forces estimated, the force induced on the actuator is estimated based on Eq. 11. Using MAPLE, the actuation distance $\rho$ for the diametrical

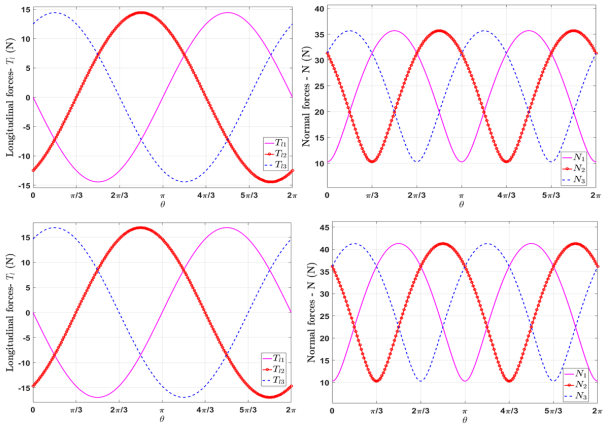


Figure 11: Forces with respect to ($\theta$) in a horizontal pipeline at $r$=37 mm for initial(above) and full extension(below) of central actuator

range of 27 mm to 37 mm was estimated to be 24 mm and 14 mm. The force transmission factor over the range of $\rho$ is estimated and the plot is shown in Fig. 12.

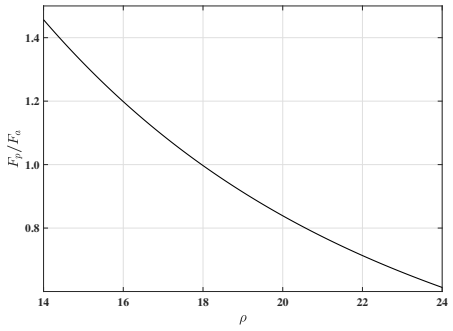


Figure 12: Force transmission factor with respect to $\rho$

Using Eq. 11 and the force transmission factor values from Fig. 12, the actuator force is calculated. In a horizontal pipeline with diameter of 27 mm, the actuator force varies from 60 N to 63 N for initial position of central actuator and from 68 N to 73 N for full extension of the central actuator. Within a diameter of 37 mm, the actuator force varies from 109 N to 113 N for initial position of central actuator and from 124 N to 129 N for full extension of the central actuator. The variation of these forces are caused by change in orientation of the robot ($\theta$) inside the pipeline. In the case of vertical orientation of the pipeline, the actuator force is constant based on the diameter of the pipeline and is not affected by the orientation of the robot. For 27 mm diameter the force is 19 N and for 37 mm diameter the force is 46 N. The results of the actuation force for the various diameters and orientation of the pipeline is provided in Fig. 13.

Higher clamping forces of around 130 N are required for the actuator when the pipe is horizontal or inclined when compared to a vertical pipeline. The moment generated by the self-weight of the robot plays an essential role on the forces generated in the actuator when traveling through horizontal pipelines. The reduction unit of the Maxon motor GP 16 S (Part number: 424749 [20]) offers a maximum static axial load of 300 N (continous) and 403 N (intermittent) which is sufficient enough for the diametrical range of pipeline under study.

## Conclusions

A bio-inspired pipeline inspection robot that mimics the motion of a caterpillar has been presented. A slot-follower mechanism is used for the legs of the robot in order to accomplish the locomotion of caterpillar. The use of this mechanism over the existing techniques like the wheeled, telescopic or pulley types makes it easier for the management of umbilicus as well as while encountering diameter changes. Also the leg mechanism makes the system lighter. With the DC motors and connecting elements, the model of the robot was made using CATIA as well as the prototype was made at LS2N, France. The static analysis on the robot helped in identifying the actuation force that was necessary for better clamping of legs on the interior walls of the pipeline. In the future, a detailed study will be made on the

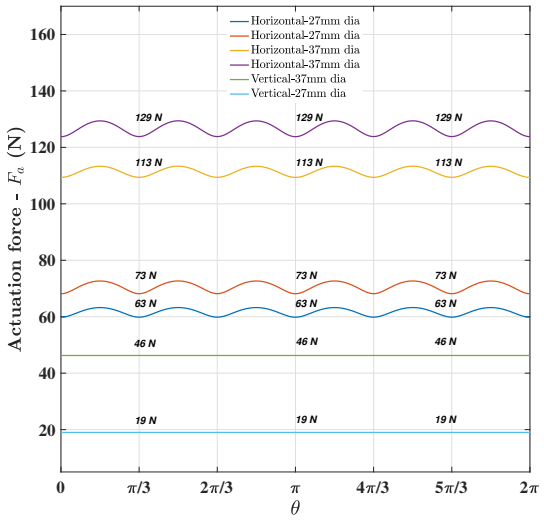


Figure 13: Variation of the actuator forces with respect to the diameter of the pipe and the orientation of the robot ($\theta$)

dynamic analysis of the robot wherein the motor torque can be computed with the help of locomotion. A Newton-Euler algorithm will be proposed for the dynamic algorithm thereby introducing feasibility for moving inside angled pipelines. Also, advanced control systems such as the EPOS2 Positioning controllers series by Maxon motors can be replaced over the existing ESCON 36/3 DC servo-controller used in the robot. The EPOS2 series have a Controller Area Network (CAN) systems which provides torque, speed and position controls from a central computer (Master) to the controllers (Slaves) installed on the robot. This system facilitates the robot to travel comparatively longer distances over the ESCON DC controllers.

## Acknowledgments

We would like to thank Daniel Kanaan, Renaud Henry and Mathieu Porez for their participation in the study of this robot. Also, we would like to express our gratitude to Stéphane Jolivet of LS2N for helping in making the prototype of the system and Benjamin Ioller for software programming.

## References

[1] I. Kassim, L. Phee, W. S. Ng, F. Gong, P. Dario, and C. A. Mosse. Locomotion techniques for robotic colonoscopy. Engineering in Medicine and Biology Magazine, 25(3):pp. 49–56, 2006.

[2] M. Takada. Self Propelled Colonoscope. *U.S. Patent 5,562,601*, 1996.

[3] S. Masuda. Apparatus for feeding a flexible tube through a conduit. *UK Patent 1,534,441*, 1978.

[4] J.M. Hyun, J.L. Hvung, M.L. Young, J.P. Juang, K. Byungkyu, and H.K. Soo. Magnetic impact actuator for robotic endoscope. In *Proc. 32nd Int. Symp. Robotics, Seoul, Korea*, pp. 1834–1838, 2001.

[5] G.J. Iddan and D. Sturlesi. In-vivo video camera. *U.S. Patent 5,604,531*, pages U.S. Patent 5,604,531, 1997.

[6] M. Drapier, V. Steenbrugghe, and B. Successeurs. Perfectionnements aux cathéters médicaux. *France Patent 1,278,965*, 1961.

[7] K. Ikuta, M. Tsukamoto, and S. Hirose. Shape memory alloy servo actuator system with electric resistance feedback and application for active endoscope. Proceedings of the IEEE International Conference on Robotics and Automation, Philadelphia, Pennsylvania, USA, April 24–29, 1988.

[8] M. Utsugi. Tubular medical instrument having a flexible sheath driven by a plurality of cuffs. *U.S. Patent 4,148,307*, 1979.

[9] M. R. Treat and W. S. Trimmer. Self-propelled endoscope using pressure driven linear actuators. *US Patent 5,595,565*, 1997.

[10] I. Ginsburgh, J. A. Carlson, G. L. Taylor, and H. Saghatchi. Method and apparatus for fluid propelled borescopes. *U.S. Patent 4,735,501*, 1988.

[11] R. Henry, D. Chablat, M. Porez, F. Boyer, D. Kanaan. MultiObjective Design Optimization of the Leg Mechanism for a Piping Inspection Robot. Proceedings of the ASME International Design Engineering Technical Conferences & Computers and Information in Engineering Conference, Buffalo, United States, 2014.

[12] R.V. Rao and G.G. Waghmare. A new optimization algorithm for solving complex constrained design optimization problems. Engineering Optimization, vol. 49, no. 1, pp. 60–83, Jan 2017.

[13] C. Anthierens, A. Ciftci, and M. Betemps. Design of an electro pneumatic micro robot for in-pipe inspection. In International Symposium on Industrial Electronics, pp. 968–972, Bled, 1999.

[14] C. Anthierens, C. Libersa, M. Touaibia, M. Betemps, M. Arsicault, and N. Chaillet. Micro robots dedicated to small diameter canalization exploration. In International Conference on Intelligent Robots and Systems, pp. 480–485, Takamatsu, 2000.

[15] Locomotion and Newton's laws. Retrieved from https://dadesai.wordpress.com on November 3, 2017.

[16] R. Rehman, S. Caro, D. Chablat, and P. Wenger. Multiobjective Design Optimization of 3-PRR Planar Parallel Manipulators. In 20th CIRP Design conference, pp. 1–10, Nantes, France, 2010.

[17] P. Valdastri, R. J.Webster, C. Quaglia, M. Quirini, A. Menciassi, and P. Dario. A New Mechanism for Mesoscale Legged Locomotion in Compliant Tubular Environments. Transactions on Robotics, 25(5): pp. 1047–1057, 2009.

[18] B. Kim, H. Y. Lim, and K. D. Kim. A locomotive mechanism for a robotic colonoscope. In International Conference on Intelligent Robots and Systems, pp. 1373–1378 vol.2, Lausanne, Switzerland, 2002.

[19] M. Quirini and R. J. Webster. Design of a pill-sized 12- legged endoscopic capsule robot. In International Conference on Robotics and Automation, pp. 10–14, Roma, 2007.

[20] Maxon motor 'Program 2017/18. High precision Drives and Systems.' Catalog retrieved from http://epaper.maxonmotor.com/, pp. 363–427, 2017.